Earth ArXiv

Topology-Preserving Multifractal Exchange Upscaling for Flow and Reactive Transport in Fractured Crystalline Rock

Qingjun Bao

Independent Researcher
Montreal, Quebec, Canada
Email: polluxbao@gmail.com

Topology-Preserving Multifractal Exchange Upscaling for Flow and Reactive Transport in Fractured Crystalline Rock

Theory, identifiability, and a proof-of-concept benchmark

Qingjun Bao

Independent Researcher, Montréal, Québec, Canada

Corresponding author: Qingjun Bao

E-mail: polluxbao@gmail.com

ORCID:

Article type: Research Article - Theoretical and Computational Methods

0.1. Highlights

- A topology-preserving multifractal exchange framework is proposed for fractured crystalline rock.
- Hydraulic multifractality, boundary-relevant topology, and matrix-exchange memory are separated explicitly.
- An upscaling objective preserves conductivity, path allocation, persistent connectivity, and exchange kernels.
- An analytically solvable graph benchmark shows that equal baseline conductance does not imply equal disturbed transport.
- A falsifiable, staged validation strategy is formulated for the Revell Batholith in northwestern Ontario.

0.2. Abstract

Flow and reactive transport in fractured crystalline rock are controlled by fracture-size distributions, aperture-dependent conductance, network connectivity, preferential pathways, matrix diffusion, and water-rock reactions. These controls are commonly represented by separate modelling components. Fractal or multifractal descriptors quantify scale-dependent heterogeneity, topological descriptors quantify connectivity and loops, and multiple-rate mass-transfer models represent exchange memory; however, a falsifiable closure that preserves these structures during upscaling remains unavailable. This study proposes a topology-preserving multifractal exchange framework (TPME) for mixed-dimensional flow and reactive transport. TPME distinguishes conductance-weighted and boundary-condition-dependent flux-weighted multifractal measures, represents robust connectivity by filtered graph or cell-complex topology, and couples the accessible fracture network to a state-conditioned distribution of fracture-matrix exchange rates. Upscaling is formulated as a multi-objective or likelihood-based problem that preserves the effective conductivity tensor, flow-path allocation, persistence diagrams, exchange transfer functions, and elemental or radionuclide mass balance. An analytically solvable four-node benchmark compares two networks with identical baseline effective conductance but different cycle rank. When one branch is disturbed, the exact effective conductance is 0.592 for the single-cycle network and 0.646 for the bridge-redundant network at a conductance multiplier of 0.101. The associated proof-of-concept particle calculation also produces different late-time quantiles and decay-weighted recovered mass, demonstrating that hydraulic redundancy does not have a universal monotonic relation with reactive transport. The framework is positioned as a testable method rather than a site prediction. A staged calibration and rejection strategy is proposed for the Revell Batholith using three-dimensional fracture observations, borehole hydraulics, conservative tracers, matrix porosity and diffusivity, mineralogy, water chemistry, and, only where identifiable, thermo-hydro-mechanical-chemical feedbacks.

Keywords: fractured crystalline rock; discrete fracture network; multifractal; persistent homology; matrix diffusion; multiple-rate mass transfer; reactive transport; radionuclide migration; upscaling; Revell Batholith

1. Introduction

Groundwater flow and solute transport in crystalline rock are frequently governed by a sparse subset of hydraulically active fractures rather than by total fracture abundance or matrix porosity alone. Fracture positions, orientations, sizes, apertures, intersections, and surface properties jointly control whether geometrical connections become effective flow paths. Broad conductance distributions can concentrate most discharge into a small hydraulic backbone, while low-permeability matrix domains store solute and produce delayed release. Consequently, an effective conductivity calibrated under one boundary condition may reproduce total flow yet fail to reproduce pathway allocation, conservative breakthrough, reactive exposure time, or response to stress- or chemistry-induced aperture change [1,2].

Fractal analysis provides a compact language for scale-dependent fracture sizes, spatial clustering, and roughness [3,4]. Multifractal analysis further distinguishes regions carrying high and low fractions of a measure and has been applied to fracture intensity in Canadian Shield rock [5]. Nevertheless, a geometrical fractal dimension does not by itself identify hydraulic accessibility. The fitted exponent also depends on finite scale range, censoring, observation window, image segmentation, and estimator choice [3]. A descriptor based only on mapped fracture pixels must therefore not be interpreted as a hydraulic multifractal unless it is weighted and tested against hydraulic observations.

Topology supplies complementary information. Node types, connected components, cycles, cut edges, and boundary accessibility distinguish networks with similar fracture density or fractal dimension [6]. Persistent homology extends this analysis by following topological features across a filtration instead of relying on one arbitrary aperture, intensity, or segmentation threshold [7-10]. Persistent topology has been used to characterize rock pores, infer fracture-forming processes, estimate flow from images, and assess single-fracture permeability [7-10]. Recent numerical work also demonstrates that artificial connections introduced during continuum upscaling can materially alter permeability and breakthrough curves [11]. These results establish that topology matters, but they do not imply a universal empirical relation between a Betti number and permeability.

For radionuclide or reactive-solute transport, fracture advection is only one component. Diffusion into connected matrix porosity, sorption or surface complexation, mineral dissolution and precipitation, aqueous speciation, and radioactive decay can strongly modify arrival and retention [12]. Multiple-rate mass transfer (MRMT) represents heterogeneous immobile-domain exchange as a distribution of rates and naturally generates memory effects [13]. Three-dimensional discrete-fracture-network studies show that flow heterogeneity, injection mode, and matrix diffusion jointly control late-time transport [14]. A central unresolved problem is therefore not whether fractal, topological, and exchange-memory effects exist separately, but how to preserve the minimum structurally relevant information when a fine fracture-matrix model is reduced to a coarser representation.

This paper proposes a topology-preserving multifractal exchange model (TPME). The framework has five contributions:

1. It distinguishes geometry-weighted, conductance-weighted, and flux-weighted multifractal measures.
2. It defines boundary-relevant filtered topology instead of using an unqualified cycle count.
3. It couples accessible fracture pathways to a state-conditioned distribution of matrix-exchange rates.
4. It defines a conservation-aware upscaling objective that preserves effective conductivity, path allocation, persistent topology, and exchange memory.
5. It establishes explicit evidence gates for upgrading a hydraulic-chemical model to hydro-mechanical or full THMC coupling.

The present contribution is a theoretical and proof-of-concept study. The numerical values are dimensionless and are not Revell Batholith predictions. Revell is used as a future validation context because the Canadian deep geological repository site has extensive geoscientific investigation and a continuing need to integrate fracture-network, hydraulic, stress, diffusion, and geochemical evidence [15,16].

2. Problem definition, hypotheses, and scope

2.1. Physical system

Let the rock domain be decomposed into a three-dimensional matrix, Ω_m, and a set of lower-dimensional fracture surfaces, Γ_f, including their intersections. At observation scale ℓ and time t, the model state is

$$\mathcal{S}(\mathbf{x}, t, \ell) = \left[\mathcal{G}_\ell, \mu_\ell, \mathcal{P}_\ell, \mathbf{z}_H, \mathbf{z}_C, \mathbf{z}_M, \mathbf{z}_T\right], \tag{1}$$

where $\mathcal{G}_\ell$ is a weighted fracture graph or cell complex, μ_ℓ is a family of spatial measures, $\mathcal{P}_\ell$ contains persistence objects, and $\mathbf{z}_H$, $\mathbf{z}_C$, $\mathbf{z}_M$, and $\mathbf{z}_T$ denote hydraulic, chemical, mechanical, and thermal state variables. Equation (1) is a bookkeeping structure and does not assume that all couplings are active.

The baseline scope is saturated or nearly saturated, single-phase flow in fractured crystalline rock with mobile fracture transport and matrix exchange. Unsaturated flow, gas generation, fracture propagation, and thermal or mechanical feedback are extensions that require additional data and identifiability tests.

Table 1. Testable hypotheses, primary observables, and rejection criteria used to evaluate the TPME framework.

Hypothesis	Scientific statement	Primary observables	Rejection criterion
H1	Networks with the same baseline effective conductance can respond differently to local aperture or conductance perturbations when their redundant paths and critical edges differ.	Effective conductivity, flow entropy, path probabilities, and breakthrough quantiles.	Topology-preserving and mean-only models are indistinguishable on held-out perturbations.
H2	A multifractal hydraulic measure is useful only over a stable finite scale range and only if it is robust to resolution, censoring, and segmentation.	Local scaling slopes, bootstrap confidence intervals, and threshold sensitivity.	Estimated spectra change arbitrarily with resolution or threshold and do not improve independent predictions.
H3	Fracture–matrix exchange must be conditioned on accessible flow, matrix diffusion length, mineralogy, and chemical state; one retardation or exchange constant is generally insufficient.	Early and late breakthrough, matrix profiles, and mineral and aqueous chemistry.	A single-rate model is equally predictive across held-out scales, flow states, and chemical events.
H4	THMC complexity is justified only when state-dependent aperture or reaction feedback exceeds observational and model uncertainty.	Stress–aperture response, temperature, and reaction-induced volume change.	Coupled feedback remains below the uncertainty of a simpler hydraulic–chemical model.

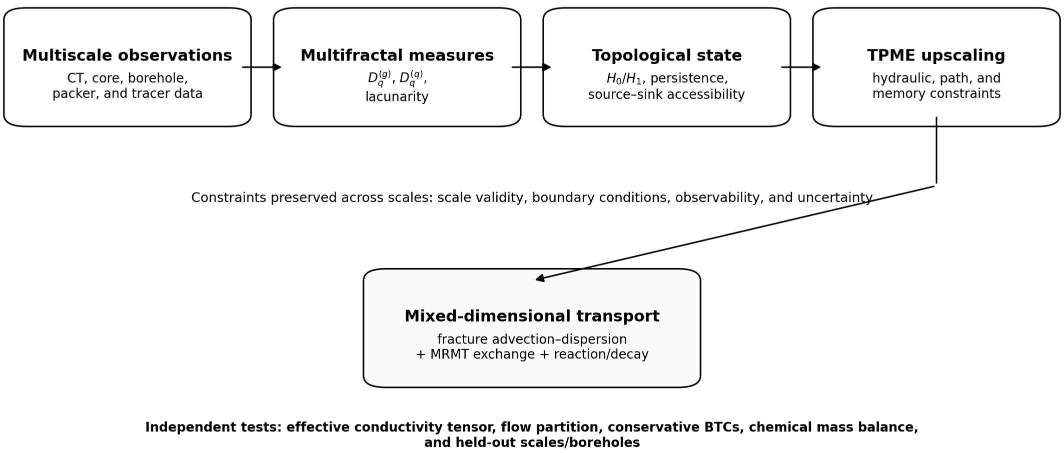

Figure 1. TPME theoretical framework. Multiscale observations are transformed into multifractal and topological descriptors that constrain TPME upscaling and mixed-dimensional transport. Independent tests are defined for conductivity, flow partition, conservative breakthrough curves (BTCs), chemical mass balance, and held-out scales or boreholes.

2.2. Testable hypotheses

3. TPME theoretical framework

3.1. Mixed-dimensional hydraulic model

For a fracture segment represented as a graph edge $e = (i, j)$, the local parallel-plate conductance is

$$g_e = \frac{w_e a_e^3}{12\mu L_e}, \qquad q_e = g_e(p_i - p_j), \tag{2}$$

where w_e is effective width, a_e is hydraulic aperture, L_e is path length, μ is dynamic viscosity, and q_e is volumetric flow. At an internal node i,

$$\sum_{e \in \delta(i)} s_{ie} q_e = Q_i, \tag{3}$$

where s_{ie} is the signed incidence coefficient. Equation (2) is a local approximation. Rough contacts, variable aperture, inertial effects, multiphase flow, and unverified aperture inversions require a resolved or calibrated hydraulic relation.

For continuum or mixed-dimensional simulation, the graph equations are replaced by Darcy flow in Ω_m and tangential Darcy or cubic-law flow on Γ_f, coupled by interface fluxes. The graph form is retained here because it makes topology and the analytical benchmark explicit.

3.2. Multifractal hydraulic measures

Three measures must be distinguished. For a box $B_k(\epsilon)$ of size ϵ,

$$\mu_k^{(A)}(\epsilon) = \frac{\sum_{e \cap B_k \neq \emptyset} A_e}{\sum_{e \in \mathcal{G}_\ell} A_e}, \qquad \mu_k^{(g)}(\epsilon) = \frac{\sum_{e \cap B_k \neq \emptyset} g_e}{\sum_{e \in \mathcal{G}_\ell} g_e}, \tag{4}$$

and, under a specified boundary condition,

$$\mu_k^{(q)}(\epsilon) = \frac{\sum_{e \cap B_k \neq \emptyset} |q_e|}{\sum_{e \in \mathcal{G}_\ell} |q_e|}. \tag{5}$$

The first measure is geometrical, the second is conductance-weighted but boundary independent, and the third identifies the active flow backbone for a particular forcing. Their partition functions are

$$Z_r^{(m)}(\epsilon) = \sum_k \left[\mu_k^{(m)}(\epsilon)\right]^r \propto \epsilon^{\tau_m(r)}, \tag{6}$$

where $m \in \{A, g, q\}$. The generalized dimensions are

$$D_r^{(m)} = \frac{\tau_m(r)}{r-1}, \quad r \neq 1, \qquad D_1^{(m)} = \lim_{\epsilon \to 0} \frac{\sum_k \mu_k^{(m)} \ln \mu_k^{(m)}}{\ln \epsilon}. \tag{7}$$

Only finite-scale estimates are physically defensible. A spectrum is accepted as a closure variable only when its local slope is stable over a predeclared range, bootstrap uncertainty is acceptable, and results are robust to observation-window and segmentation changes.

3.3. Boundary-relevant topology and persistence

For a graph, the cycle rank is

$$\beta_1 = |E| - |V| + \beta_0, \tag{8}$$

where β_0 is the number of connected components. Equation (8) is not a substitute for homology of a three-dimensional fracture-surface complex, which may also contain two-dimensional cavities and requires explicit construction of a cell or simplicial complex.

A weighted filtration is defined by a normalized hydraulic threshold θ:

$$\mathcal{K}_\theta = \{e \in E : \hat{g}_e \geq \theta\} \cup V(\theta), \tag{9}$$

or, for boundary-conditioned analysis, by $\widehat{|q_e|}$. Persistence diagrams $\mathcal{P}_0$ and $\mathcal{P}_1$ record the birth and death of connected components and loops. For transport, source-to-sink accessibility must also be tracked:

$$\Pi_{ST}(\theta) = \begin{cases} 1, & S \text{ and } T \text{ are connected in } \mathcal{K}_\theta, \\ 0, & \text{otherwise.} \end{cases} \tag{10}$$

Relative homology or an equivalent boundary-connectivity persistence construction is preferable when the scientific quantity is entry-to-exit transport rather than internal loop abundance. Cut edges, articulation points, and minimum hydraulic cuts provide additional interpretable measures of fragility.

3.4. Fracture-matrix transport and multiple-rate exchange

For species i on a fracture surface, the mobile storage per fracture area is $\omega_f C_{f,i}$, with $\omega_f = a\phi_f$. The mixed-dimensional balance is

$$\frac{\partial(\omega_f C_{f,i})}{\partial t} + \nabla_\tau \cdot \left(\mathbf{q}_f C_{f,i} - \omega_f \mathbf{D}_f \nabla_\tau C_{f,i}\right) = -J_{fm,i} + R_{f,i}. \tag{11}$$

Instead of absorbing heterogeneous matrix processes into one retardation factor, define a non-negative exchange-storage density $\rho(\alpha \mid \mathcal{S})$ such that

$$\int_0^\infty \rho(\alpha \mid \mathcal{S})\, d\alpha = \omega_{im}, \tag{12}$$

where ω_{im} is total accessible immobile storage per fracture area. The exchange flux is

$$J_{fm,i}(t) = \int_0^\infty \alpha \left[C_{f,i}(t) - C_{\alpha,i}(t)\right] \rho(\alpha \mid \mathcal{S})\, d\alpha, \tag{13}$$

with

$$\frac{\partial C_{\alpha,i}}{\partial t} = \alpha(C_{f,i} - C_{\alpha,i}) - \lambda_i C_{\alpha,i} + R^{chem}_{\alpha,i}. \tag{14}$$

If $C_{\alpha,i}(0) = 0$ and chemistry and decay are temporarily omitted, Laplace transformation gives

$$\widetilde{C}_{\alpha,i}(s) = \frac{\alpha}{s+\alpha}\widetilde{C}_{f,i}(s), \tag{15}$$

and therefore

$$\widetilde{J}_{fm,i}(s) = \underbrace{\left[\int_0^\infty \frac{\alpha s}{s+\alpha}\rho(\alpha \mid \mathcal{S})\,d\alpha\right]}_{\widetilde{K}_{fm}(s|\mathcal{S})}\widetilde{C}_{f,i}(s). \tag{16}$$

The transfer function $\widetilde{K}_{fm}$ is the exchange-memory kernel. TPME does not prescribe $\alpha = f(D_r, \beta_1)$. Instead, a hierarchical conditional model may be calibrated:

$$\ln \alpha_e = h\big(\ln |q_e|, a_e, d_{m,e}, \zeta_e, \mathbf{z}_C\big) + \xi_e, \tag{17}$$

where $d_{m,e}$ is accessible matrix diffusion length, ζ_e describes mineral or surface class, and ξ_e represents unresolved heterogeneity. Multifractal and topological descriptors constrain pathway accessibility and flux allocation; they do not replace diffusion distance, mineralogy, or aqueous chemistry.

3.5. Reaction, decay chains, and conservation

For a decay chain, aqueous, mineral, and sorbed reaction terms must be combined with a decay-production matrix. In vector form,

$$\mathbf{R}_f = \mathbf{R}^{aq} + \mathbf{R}^{min} + \mathbf{R}^{sorp} + \omega_f \mathbf{A}_d \mathbf{C}_f, \tag{18}$$

where diagonal entries of $\mathbf{A}_d$ are $-\lambda_i$ and off-diagonal entries contain branching production from parent nuclides. The reaction network must be tied to measured pH, alkalinity, dissolved inorganic carbon, redox indicators, major ions, mineralogy, filtered and unfiltered radionuclide analyses, and a documented thermodynamic database. A universal distribution coefficient must not replace speciation and surface evidence when those processes are material to the prediction.

The numerical ledger for each conserved element or radionuclide chain is

$$M_i^0 + M_i^{in} = M_i^{out} + M_i^{f,mob} + M_i^{m,aq} + M_i^{sorbed} + M_i^{mineral} + M_i^{decayed} + \varepsilon_i^{num}. \tag{19}$$

Reversible reactions are represented by current inventories rather than by an ambiguous cumulative "reacted" term. Equation (19) is a stronger test than matching one breakthrough peak because it can expose errors in flow, exchange, reaction, or decay implementation.

3.6. Topology-preserving upscaling objective

Let subscripts f and c denote fine and coarse models. For symmetric positive-definite conductivity tensors, use the log-Euclidean distance

$$d_K(\mathbf{K}_c, \mathbf{K}_f) = \left\|\log \mathbf{K}_c - \log \mathbf{K}_f\right\|_F. \tag{20}$$

A normalized TPME model-selection objective over a finite observational frequency band is

$$\begin{aligned}\mathcal{J}_{TPME} = w_K \hat{d}_K + w_q D_{JS}(\pi_f, \pi_c) + w_P \widehat{W}_p(\mathcal{P}_f, \mathcal{P}_c) \\ + w_M \int_{\omega_{min}}^{\omega_{max}} \left| \widehat{K}_{fm,c}(i\omega) - \widehat{K}_{fm,f}(i\omega) \right|^2 d \ln \omega + w_B \hat{\mathcal{E}}_{balance},\end{aligned} \tag{21}$$

where D_{JS} compares aligned path or edge-flow distributions, W_p is a Wasserstein or bottleneck distance between persistence diagrams, and hats denote normalization by predeclared reference scales. The frequency interval must correspond to the experiment or prediction horizon; an unbounded integral is neither identifiable nor numerically necessary.

The weights in Equation (21) should not be selected solely to improve training fit. Preferred options are (i) a likelihood in which each residual is scaled by observational covariance, (ii) Bayesian hierarchical inversion, or (iii) preregistered cross-validation and Pareto analysis. If a structural term does not improve held-out hydraulic or transport prediction, it is rejected from the closure.

3.7. Evidence-based upgrade to THMC

A hydraulic-chemical model is upgraded only when mechanical, thermal, or chemical aperture feedback is observable. A candidate aperture law is

$$a_e(t) = a_{r,e} + \left(a_{0,e} - a_{r,e}\right) \exp\left[-\frac{\sigma'_{n,e}(t)}{\sigma_{c,e}}\right] + \Delta a_{shear,e} - \frac{\Delta V_{precip,e} - \Delta V_{diss,e}}{A_{f,e}}, \tag{22}$$

where a_r is residual aperture, σ'_n is effective normal stress, σ_c is a closure scale, and mineral-volume change is converted to aperture by fracture area. Because $g_e \propto a_e^3$, small aperture changes can reorganize flow and exchange. Nevertheless, if stress-aperture, temperature, or reaction feedback is smaller than measurement and model uncertainty, the simpler HC model is retained.

4. Analytical and numerical proof-of-concept benchmark

4.1. Network definition

Two four-node networks contain source s, sink t, and two parallel branches through nodes a and b (Figure 2). All branch-edge conductances are unity except $g_{sa} = \eta$. Network B additionally contains bridge edge a—b with conductance $h = 0.6$. At $\eta = 1$, both networks have dimensionless effective conductance $K^* = 1$. Network A has $\beta_1 = 1$ and Network B has $\beta_1 = 2$.

The local change in η is an abstract conductance perturbation. It is not assigned to stress closure, precipitation, dissolution, or any field parameter.

4.2. Exact hydraulic solution

For Network A, the two branches act in parallel, giving

$$K_A^*(\eta) = \frac{1}{2} + \frac{\eta}{1+\eta}. \tag{23}$$

Solving the two internal-node balance equations for Network B gives

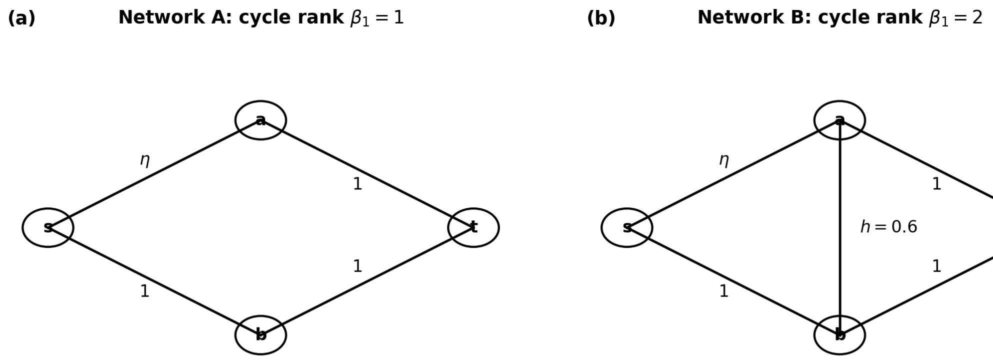

Figure 2. Analytically solvable benchmark networks used in Section 4.1: (a) Network A with cycle rank $\beta_1 = 1$ and (b) Network B with cycle rank $\beta_1 = 2$. Edge labels denote dimensionless conductances.

$$K_B^*(\eta, h) = \frac{2\eta h + 3\eta + 2h + 1}{\eta h + 2\eta + 3h + 2}. \tag{24}$$

Both equations return unity at $\eta = 1$. With $h = 0.6$ and $\eta = 0.101$,

$$K_A^* = 0.5917, \qquad K_B^* = 0.6459. \tag{25}$$

At $\eta = 0.05$, the corresponding values are 0.5476 and 0.6132. Thus the redundant bridge is hydraulically inactive when the network is symmetric but becomes valuable after a local perturbation.

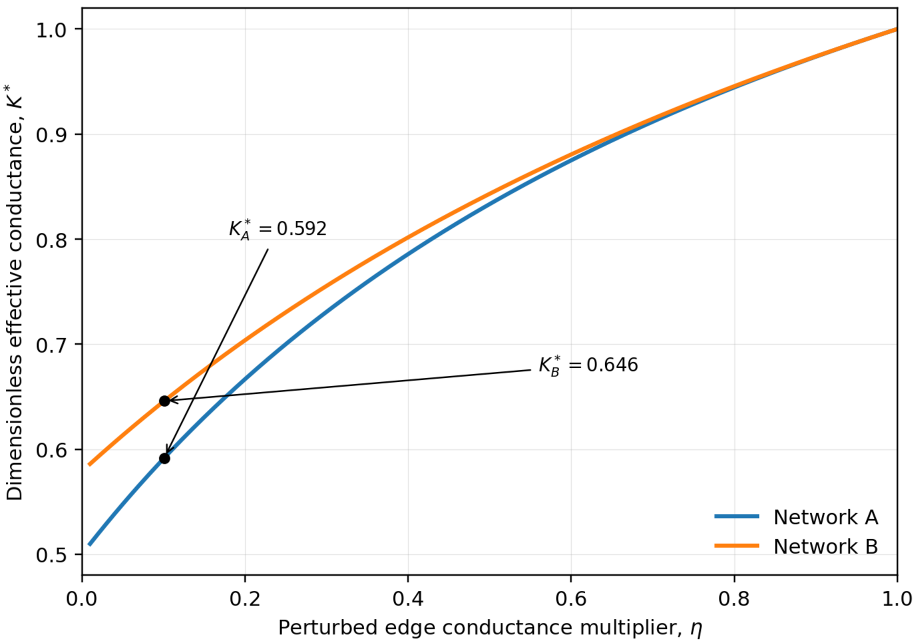

Figure 3. Exact dimensionless effective conductance under a local edge-conductance perturbation, parameterized by the multiplier η in Equations (23) and (24).

4.3. Proof-of-concept transport calculation

The original proof-of-concept transport calculation used flow-weighted path selection, one prescribed random fracture-matrix delay, 6000 particles per state, and a fixed seed of 20260726. A dimensionless decay weight $\exp(-\lambda^* t^*)$ with $\lambda^* = 0.03$ was used only to expose the interaction between pathway selection, exchange delay, and residence time; it does not represent a specific radionuclide.

At $\eta \approx 0.101$, the reported diagnostics were:

Table 2. Diagnostic metrics reported for the dimensionless proof-of-concept transport calculation at $\eta \approx 0.101$.

Metric	Network A, $\beta_1 = 1$	Network B, $\beta_1 = 2$	Interpretation
K^*	0.592	0.646	Exact hydraulic response.
Flow entropy H_Q	0.811	0.867	Bridge redistributes accessible flow.
t^*_{90}	23.74	18.11	Conditional late-arrival quantile.
Mean decay-weighted recovered fraction	0.812	0.785	More hydraulic redundancy does not imply greater survival.

The hydraulic values are reproduced analytically by Equations (23)-(25). The stochastic transport values demonstrate internal distinguishability but are not sufficient for field inference. Before journal claims are extended beyond proof of concept, the particle algorithm, delay distribution, convergence, random-seed sensitivity, and confidence intervals must be included in a public supplement.

4.4. Interpretation

The benchmark establishes three points. First, matching one baseline K^* does not ensure equivalent response under a changed state. Second, β_1 alone does not determine the magnitude of that response; bridge weight, boundary condition, and location matter. Third, faster late-time arrival can coexist with lower decay-weighted recovery because the bridge changes both travel paths and exchange exposure. Therefore, topology is a conditional structural variable rather than a universal monotonic proxy for transport.

5. Revell Batholith validation strategy

The Revell Batholith in northwestern Ontario is the selected location for Canada's used nuclear fuel deep geological repository and has been investigated through deep boreholes, core characterization, hydraulic testing, geophysics, stress analysis, groundwater chemistry, and site-scale modelling [15,16]. The present manuscript does not use proprietary or unreleased Revell data and makes no repository safety conclusion. Revell is used to define a realistic validation programme.

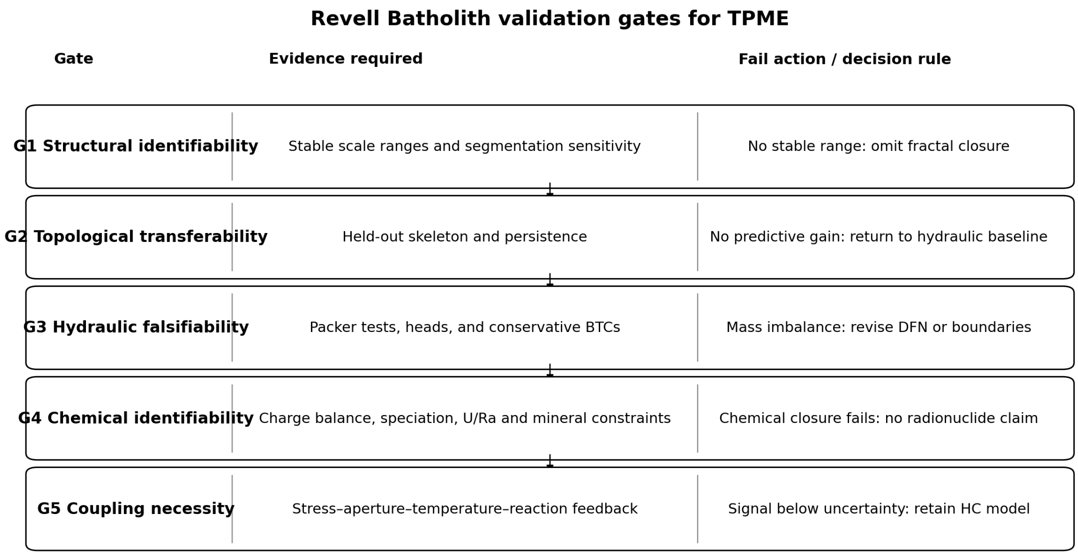

Figure 4. Revell Batholith validation gates for TPME. Progression to more complex closure assumptions is permitted only when the evidence requirement is met; otherwise, the stated fail action is taken.

5.1. Gate G1: structural identifiability

A versioned three-dimensional fracture dataset should record coordinates, depth reference, observation method, resolution, censoring, fracture set, confidence, and processing history. Borehole and outcrop observations require stereological correction and explicit observation models. The following are tested before any fractal closure is accepted:

- finite-scale ranges for length, spacing, intensity, aperture, and conductance measures;
- bootstrap uncertainty of D_r and $f(\alpha)$;
- segmentation, censoring, and window sensitivity;
- consistency across core, borehole imaging, geophysics, and mapped fracture domains.

If no stable scale range exists, the corresponding multifractal descriptor is not used.

5.2. Gate G2: topological transferability

A family of posterior DFN realizations is generated rather than one "true" network. Topological targets include boundary accessibility, persistence of connected backbones, cycle structure, cut edges, and intersection statistics. The model is tested on held-out boreholes, fracture domains, or observation scales. If topological descriptors do not improve transfer beyond conventional DFN statistics, the additional constraint is rejected.

5.3. Gate G3: hydraulic and conservative-transport falsification

Packer tests, pressure interference, heads, flow logging, and conservative tracers are used to calibrate aperture or transmissivity distributions and boundary conditions. TPME is compared under identical forcing against:

1. high-resolution DFN or mixed-dimensional flow;
2. equivalent-continuum upscaling without topology preservation;

3. dual-porosity or dual-permeability models;
4. MRMT transport without multifractal or topological constraints.

Required outputs include conductivity tensor, pressure, boundary flux, first-arrival time, quantiles, late-time slope, and full mass balance. Improvement must be demonstrated on held-out data rather than only calibration data.

5.4. Gate G4: geochemical and radionuclide identifiability

Reactive transport begins with a documented aqueous and mineral mass balance. Measurements should include pH, temperature, alkalinity, dissolved inorganic carbon, major ions, Fe/Mn redox indicators, sulphide where relevant, filtered/unfiltered U and Ra, mineralogy, surface area, matrix porosity, and effective diffusion coefficients. Aqueous speciation and mineral saturation screening can be performed using PHREEQC or an equivalent verified module before coupling to a transport simulator. Database version, activity model, selected outputs, and reaction assumptions must be archived.

The purpose of the chemistry gate is not to force every possible reaction into the model. It is to identify which reactions are observable and necessary, and to reject radionuclide interpretations when charge balance, redox evidence, or mineral constraints are inadequate.

5.5. Gate G5: THMC necessity

Mechanical and thermal coupling is introduced only if it improves prediction of pressure, aperture, conductivity, tracer response, or mineral-volume change beyond uncertainty. Candidate data include in situ stress, core mechanical properties, fracture-normal closure, shear dilation, thermal properties, and reaction-induced aperture changes. The hierarchy is therefore HC $\rightarrow$ HMC/THC $\rightarrow$ THMC, not automatic full coupling.

6. Discussion

6.1. Scientific value and novelty

The primary contribution is not a new claim that fractures are fractal or that topology influences flow. Both are established [3-11]. The contribution is an explicit closure architecture in which scale-dependent hydraulic measures, boundary-relevant topology, and exchange memory are preserved and tested together. This architecture addresses four deficiencies of mean-only upscaling:

- equal effective conductivity can conceal different response to local state change;
- geometrical connectivity can conceal a sparse active hydraulic backbone;
- transport memory can be altered even when total flow is preserved;
- reactive or decay-weighted outputs can vary non-monotonically with hydraulic redundancy.

The analytical benchmark also improves the theoretical basis of the original concept by separating an exact hydraulic result from a stochastic transport illustration.

6.2. Relation to existing approaches

TPME is compatible with established mixed-dimensional and DFN formulations rather than replacing them [2,17,18]. It differs from single-index fractal models because it distinguishes geometric, conductance, and active-flux measures. It differs from direct topology-to-permeability regression because persistence is used as a preserved structural constraint that still requires hydraulic validation. It extends MRMT conceptually by conditioning exchange-rate distributions on accessible network state while retaining independent matrix and chemical variables [13,14].

The framework is particularly relevant where no clean representative elementary volume exists. In such systems, averaging may preserve mean flow while creating false connections or destroying bottlenecks [11]. TPME cannot eliminate non-uniqueness, but it can narrow the set of admissible coarse models by retaining observably relevant structure.

6.3. Identifiability and uncertainty

Different fracture geometries can produce similar pressure and breakthrough data. The model should therefore infer posterior ensembles rather than a unique network. Uncertainty sources include:

- one- or two-dimensional sampling of three-dimensional fracture surfaces;
- finite resolution and unobserved small apertures;
- non-unique inversion from transmissivity to aperture;
- boundary-condition uncertainty;
- sensitivity of persistence to filtration and edge construction;
- matrix diffusion-length and accessible-porosity uncertainty;
- thermodynamic-database and surface-complexation uncertainty;
- long-term climate, stress, and chemical scenarios.

Bayesian calibration, simulation-based inference, or ensemble smoothing can propagate these uncertainties. Predictive skill should be reported with coverage probabilities and proper scoring rules, not only deterministic error.

6.4. Applicability and boundaries

TPME is most appropriate when:

- a fracture network or pore network can be reconstructed probabilistically;
- hydraulic or tracer observations exist to weight structural measures;
- matrix exchange produces measurable memory;
- the coarse model is intended to retain response over a specified scale and frequency band.

It is not justified when data support only a homogeneous continuum, when the fitted fractal range is unstable, or when topological features are dominated by imaging artifacts. The current formulation assumes single-phase flow and does not address unsaturated phase topology, gas generation, fracture propagation, or colloid-facilitated transport. Those require separate extensions.

6.5. Research programme required for full validation

A publishable and defensible research programme should progress through four levels:

1. **Synthetic ensembles.** Generate hundreds to thousands of three-dimensional truncated power-law and clustered DFNs. Compare mean-only, topology-preserving, and full DFN models across density, aperture contrast, stress perturbation, and matrix-exchange distributions.
2. **Laboratory experiments.** Use rough single fractures and fractured cores with micro-CT or surface scanning, pressure/flow measurements, conservative tracers, and matrix

concentration profiles. Test filtration stability and exchange-kernel recovery.

3. **Revell calibration.** Build a probabilistic site DFN from authorized borehole, core, hydraulic, diffusion, geochemical, and stress data. Use grouped holdout by borehole and fracture domain.
4. **Long-term radionuclide scenarios.** Couple only validated processes; quantify arrival-time distributions, peak concentration, late-time release, decay-chain inventories, and scenario/model uncertainty over repository-relevant horizons.

7. Limitations

1. The benchmark contains four nodes and does not establish performance for realistic three-dimensional DFNs.
2. The transport calculation is a dimensionless proof of concept and is not a substitute for a verified mixed-dimensional transport solver.
3. No Revell field inversion, site tracer fit, radionuclide speciation, or safety assessment is reported.
4. The persistence filtration, objective weights, and observational frequency band must be selected and tested for each application.
5. Long-term extrapolation requires scenario and structural uncertainty; short-time scale relations cannot be assumed valid over centuries without mechanistic evidence.
6. The manuscript does not yet provide the public repository, raw synthetic particle output, or automated regression tests expected for a computational methods paper. These are pre-submission requirements.

8. Conclusions

A topology-preserving multifractal exchange framework has been developed for upscaling flow and reactive transport in fractured crystalline rock. The framework separates hydraulic multifractality from geometry, represents boundary-relevant topology through filtered connectivity and persistence, and embeds heterogeneous matrix exchange in a state-conditioned memory kernel. It also corrects a common conceptual error: neither fractal dimension nor cycle rank is a direct substitute for permeability, reaction rate, or radionuclide retardation.

The four-node benchmark provides an exact demonstration that two networks with equal baseline effective conductance can have different disturbed conductance. With a bridge conductance of 0.6 and a perturbed-edge multiplier of 0.101, the exact effective conductances are 0.592 and 0.646. The accompanying illustrative transport calculation shows that this hydraulic advantage can coexist with different late-time arrival and lower decay-weighted recovery. Topological redundancy is therefore state and process dependent.

The value of TPME for the Revell Batholith lies in its staged falsification strategy, not in an uncalibrated site prediction. Structural descriptors must first be scale-stable; topology must transfer to held-out observations; hydraulic and conservative transport must close; chemistry must be independently constrained; and THMC coupling must demonstrate measurable benefit. If these gates are not passed, the model must revert to a simpler representation.

9. Data and code availability

The hydraulic benchmark is analytically reproducible from Equations (23) and (24). Before submission, the particle-transport script, environment file, random seeds, derived tables, and figure-generation scripts should be deposited in a versioned public repository and archived with a DOI. No proprietary or unreleased Revell Batholith data are included in this manuscript.

10. Author contribution

Qingjun Bao: Conceptualization, methodology, formal analysis, investigation, writing - original draft, writing - review and editing, visualization.

11. Competing interests

The author declares no competing interests.

12. Funding

No external funding was received for the theoretical work reported in this manuscript.

13. Acknowledgements

The author acknowledges the foundational work of researchers in fractal soil mechanics, discrete fracture networks, persistent homology, matrix diffusion, and multiple-rate mass transfer. Any institutional or data-provider acknowledgements required for future Revell application should be added only after data access and contribution terms are confirmed.

14. References

[**1**] Berkowitz, B. (2002). Characterizing flow and transport in fractured geological media: A review. *Advances in Water Resources*, 25, 861-884. https://doi.org/10.1016/S0309-1708(02)00042-8

[**2**] Berre, I., Doster, F., & Keilegavlen, E. (2019). Flow in fractured porous media: A review of conceptual models and discretization approaches. *Transport in Porous Media*, 130, 215-236. https://doi.org/10.1007/s11242-018-1171-6

[**3**] Bonnet, E., Bour, O., Odling, N. E., Davy, P., Main, I., Cowie, P., & Berkowitz, B. (2001). Scaling of fracture systems in geological media. *Reviews of Geophysics*, 39, 347-383. https://doi.org/10.1029/1999RG000074

[**4**] Perrier, E., Bird, N., & Rieu, M. (1999). Generalizing the fractal model of soil structure: The pore-solid fractal approach. *Geoderma*, 88, 137-164. https://doi.org/10.1016/S0016-7061(98)00102-5

[**5**] Agterberg, F. P., Cheng, Q., Brown, A., & Good, D. (1996). Multifractal modeling of fractures in the Lac du Bonnet Batholith, Manitoba. *Computers & Geosciences*, 22, 497-507. https://doi.org/10.1016/0098-3004(95)00117-4

[**6**] Sanderson, D. J., & Nixon, C. W. (2015). The use of topology in fracture network characterization. *Journal of Structural Geology*, 72, 55-66. https://doi.org/10.1016/j.jsg.2015.01.005

[**7**] Jiang, F., Tsuji, T., & Shirai, T. (2018). Pore geometry characterization by persistent homology theory. *Water Resources Research*, 54, 4150-4163. https://doi.org/10.1029/2017WR021864

[**8**] Suzuki, A., Miyazawa, M., Okamoto, A., Shimizu, H., Obayashi, I., Hiraoka, Y., Tsuji, T., Kang, P. K., & Ito, T. (2020). Inferring fracture forming processes by characterizing fracture network patterns with persistent homology. *Computers & Geosciences*, 143, 104550. https://doi.org/10.1016/j.cageo.2020.104550

[**9**] Suzuki, A., Miyazawa, M., Minto, J. M., Tsuji, T., Obayashi, I., Hiraoka, Y., & Ito, T. (2021). Flow estimation solely from image data through persistent homology analysis. *Scientific Reports*, 11, 17948. https://doi.org/10.1038/s41598-021-97222-6

[**10**] Fuchs, M., Suzuki, A., Hasumi, T., & Blum, P. (2024). Investigating rough single-fracture permeabilities with persistent homology. *Solid Earth*, 15, 353-365. https://doi.org/10.5194/se-15-353-2024

[**11**] Pachalieva, A. A., Sweeney, M. R., Viswanathan, H., Stein, E., Leone, R., & Hyman, J. D. (2023). Impact of artificial topological changes on flow and transport through fractured media due to mesh resolution. *Computational Geosciences*, 27, 1145-1163. https://doi.org/10.1007/s10596-023-10253-y

[**12**] Neretnieks, I. (1980). Diffusion in the rock matrix: An important factor in radionuclide retardation? *Journal of Geophysical Research*, 85, 4379-4397. https://doi.org/10.1029/JB085iB08p04379

[**13**] Haggerty, R., & Gorelick, S. M. (1995). Multiple-rate mass transfer for modeling diffusion and surface reactions in media with pore-scale heterogeneity. *Water Resources Research*, 31, 2383-2400. https://doi.org/10.1029/95WR10583

[**14**] Hyman, J. D., & Dentz, M. (2021). Transport upscaling under flow heterogeneity and matrix diffusion in three-dimensional discrete fracture networks. *Advances in Water Resources*, 155, 103994. https://doi.org/10.1016/j.advwatres.2021.103994

[**15**] Nuclear Waste Management Organization. (2025). *Report of the NWMO Adaptive Phased Management Geoscientific Review Group: Annual Report 2024*. Toronto, Canada.

[**16**] Nuclear Waste Management Organization. (2026). *Site selection: Revell Batholith, northwestern Ontario*. NWMO public project information.

[**17**] Berre, I., Boon, W. M., Flemisch, B., et al. (2021). Verification benchmarks for single-phase flow in three-dimensional fractured porous media. *Advances in Water Resources*, 147, 103759. https://doi.org/10.1016/j.advwatres.2020.103759

[**18**] Flemisch, B., Berre, I., Boon, W., et al. (2018). Benchmarks for single-phase flow in fractured porous media. *Advances in Water Resources*, 111, 239-258. https://doi.org/10.1016/j.advwatres.2017.10.0

[**19**] Sund, N. L., Parashar, R., & Pham, H. V. (2021). Upscaling of transport through discrete fracture networks via random walk: A comparison of models. *Physical Review E*, 103, 062116. https://doi.org/10.1103/PhysRevE.103.062116

[**20**] Gascoyne, M. (1989). High levels of uranium and radium in groundwaters at Canada's Underground Research Laboratory, Lac du Bonnet, Manitoba, Canada. *Applied Geochemistry*, 4, 577-591. https://doi.org/10.1016/0883-2927(89)90068-1

[**21**] Xu, Y. (2026). *Fractal Soil Mechanics*. Elsevier. ISBN 978-0-443-44470-8.

[**22**] Rieu, M., & Sposito, G. (1991). Fractal fragmentation, soil porosity, and soil water properties. *Soil Science Society of America Journal*, 55.

[**23**] Cohen-Steiner, D., Edelsbrunner, H., & Harer, J. (2007). Stability of persistence dia-

grams. *Discrete & Computational Geometry*, 37, 103-120. https://doi.org/10.1007/s00454-006-1276-5

[24] Edelsbrunner, H., & Harer, J. (2010). *Computational Topology: An Introduction.* American Mathematical Society.

[25] Keilegavlen, E., Fumagalli, A., Berge, R., & Stefansson, I. (2019). Implementation of mixed-dimensional models for flow in fractured porous media. *Computational Geosciences*, 23, 685-701. https://doi.org/10.1007/s10596-018-9797-4